One-dimensional and two-dimensional arrays of nanoholes generated by laser in the semiconfined configuration

S. Lugomer[a] and A. Maksimović
Ruđer Bošković Institute, Bijenička c. 54, 10001 Zagreb, Croatia

G. Peto, A. Toth, and E. Horvath
Research Institute for Technical Physics and Material Sciences, Hungarian Academy of Sciences, P.O.B 49, H-1525 Budapest, Hungary

(Received 20 December 2005; accepted 18 September 2006; published online 17 November 2006)

We have shown that nanoporosity can be generated on metal surfaces by nanosecond laser-matter interactions in the semiconfined configuration. The scanning electron microscope analysis has shown that nanoholes of ~25–50 nm in diameter, arranged in one-dimensional (1D) and two-dimensional (2D) irregular and regular arrays, have been formed. The interpretation is based on the generation of a dispersive, dissipative system of nonlinear solitary plasma waves (humps) that leave temperature/pressure fingerprints on the metal surface. It has been shown that the 1D irregular array of nanoholes can be interpreted as a result of the irregular string of solitary humps obtained by numerical simulation based on the Benney pd equation with the Gaussian perturbation. The 2D random array of nanoholes can be interpreted as a result of random solitary humps that can be obtained by numerical simulation from the Benney equation with the periodic perturbation. The regular string of nanoholes has been shown to appear as a result of breather modes (bound state of solitons), the numerical simulation of which has been based on the Boussinesq equation. The regular 2D array of nanoholes has been interpreted as fingerprints of breather modes, in agreement with the result of the numerical simulation of Tajiri and Murakami, [J. Math. Phys. **34**, 2400 (1993)], based on the Kadomtsev-Petviashvili equation. © *2006 American Institute of Physics*.
[DOI: 10.1063/1.2388122]

I. INTRODUCTION

The generation of nanoholes in the specific type of arrangement that was observed in some domains of the micro-scale porous surface and briefly mentioned in the previous paper by Lugomer *et al.*[1] is an intriguing phenomenon. Observed in the special experimental configuration called semiconfined (SCC), these morphologic characteristics require an in-depth study. Besides the fundamental importance for plasma dynamics, the generation of nanoholes in one-dimensional (1D) and two-dimensional (2D) arrays is of great importance for various kinds of technological applications.

Metal surfaces of micron-scale porosity are produced in laser ablation performed in the experimental configuration that we call semiconfined.[1,2] In this configuration, a laser beam illuminates the target through a transparent cover plate positioned slightly above the target. The ablated plasma has a very limited space to expand, so that the pressure increases driving the liquid surface layer into the superheated state. Consequently, the boiling temperature T_B is shifted to higher $T_{B'}$, and at the moment when the plasma disk reaches the detonation threshold, the explosion occurs, generating a cylindrical blast wave.[3,4] The abrupt increase of pressure pushes the superheated liquid layer toward the spinodal (the point of absolute thermodynamic instability), and triggers the explosive phase transition of the spinodal fluid into the gaseous phase through a cascade of babblings and bubble explosions. Bubble explosions form a very porous, spongelike target surface morphology.[1] The scanning electron microscopy (SEM) analysis reveals that the micron-scale convex surface domains of the spongelike surface comprise 1D and 2D irregular as well as regular arrays of nanoholes, mentioned briefly in Ref. 1.

This paper presents the results of an in-depth study of this phenomenon. The crucial fact is that nanoholes are observed only in the semiconfined configuration of light-matter interaction (LMI) because of the generation of solitary plasma waves. We assume that the origin of the solitary waves is the blast wave reflected from the transparent cover plate, which causes the piston effect on the plasma density interface.[5] Behind the shock wave, the plasma instabilities start to grow in the form of density oscillations that evolve into ion acoustic solitary waves.[5] However, the irregular spongelike surface morphology induced by the spinodal explosion result to the piston effect having different consequences in different target domains. Thus, the origin of regular and irregular nanoporosities lies in the characteristics of solitary plasma waves and their interaction with the target surface.

The detailed SEM analysis of the convex parts of a porous surface reveals holes from ~25 to 50 nm (or more) in diameter, which appears as 1D string, 2D quasiregular arrays, or finally, as regular parallel arrays of holes. We attribute their origin to dispersive hump solitons, as well as to the so-called "breather modes" of the target plasma. Repre-

[a]Electronic mail: lugomer@irb.hr

senting compressive waves, they form nanoholes as fingerprints of the temperature/pressure effect on various parts (domains) of a target surface. The fingerprints remain frozen permanently at the end of the laser pulse, because of ultrafast cooling. Various types of nanohole organization are favorably compared with the results of the numerical simulation based on the Benney and on the Boussinesq pd equation.

II. EXPERIMENT

The experiments were performed using a single pulse of a Q-switched Nd:YAG (yttrium aluminium garnet) laser ($E_s \sim 10\ J/cm^2$, $P_s \sim 2.5\times10^8\ W/cm^2$, $\tau=40$ ns, $\lambda=1.06\ \mu m$). A matte molybdenum plate of $1\times1\times0.1\ cm^3$, a very hard material with high melting and boiling points, was used as target. To generate conditions of very high temperature and pressure, the target was illuminated in the semiconfined configuration, through a transparent quartz plate positioned 300–500 μm above the target surface.

The ablated plasma is effectively trapped between the target surface and the cover plate. For this reason, the plasma pressure increases, driving the liquid surface layer into the superheated state, i.e., into the metastable liquid phase. At the moment when the plasma disk reaches the detonation threshold, the explosion occurs, thus generating a disklike cylindrical blast wave.[1–4]

The radius of the blast wave for molybdenum targets was found to range from $R \sim 2800$ to 3300 μm, depending on the laser energy. It travels at the supersonic velocity of $\sim10^6$ cm/s and increases the pressure up to ~30 kbars ($\sim30\times10^3$ atm)—roughly estimated on the literature basis.[6,7]

The formation of the blast wave initiates two simultaneous processes: one in the plasma density interface (ρ_H/ρ_L) and the other in the superheated liquid layer.

Perturbation of the plasma density interface by the piston effect. The process taking place in the plasma slab is schematically shown in Figs. 1(a)–1(f). The blast wave formed by the plasma explosion has an expanding hemispherical shape [Fig. 1(a)] and reaches the cover plate [Fig. 1(b)]. Reflected back toward the metal surface, it strikes the high-density/low-density (ρ_H/ρ_L) interface and snow plows the background plasma [Figs. 1(c) and 1(d)].[8] Behind the shock, the plasma density interface is modulated, which leads to instability characteristic of the piston effect [Fig. 1(e)].[5] The scenario presented in Figs. 1(a)–1(f) shows that the piston perturbation of the interface causes plasma density oscillations. They represent fluid waves that travel perpendicularly to the density gradient direction, i.e., horizontally between two plates [Fig. 1(f)].

Perturbation of the plasma interface by bubble explosions. The very high peak pressure generated by the blast wave causes the superheating of the liquid surface layer and the formation of a metastable state.[11] The superheating is much higher for the matte targets than for the smooth ones and may reach the spinodal, the point of absolute thermodynamic instability.[12] The transition from the superheated fluid into vapor occurs through abrupt bubble nucleation and the phase explosion (PE). The PE of spinodal fluid associated

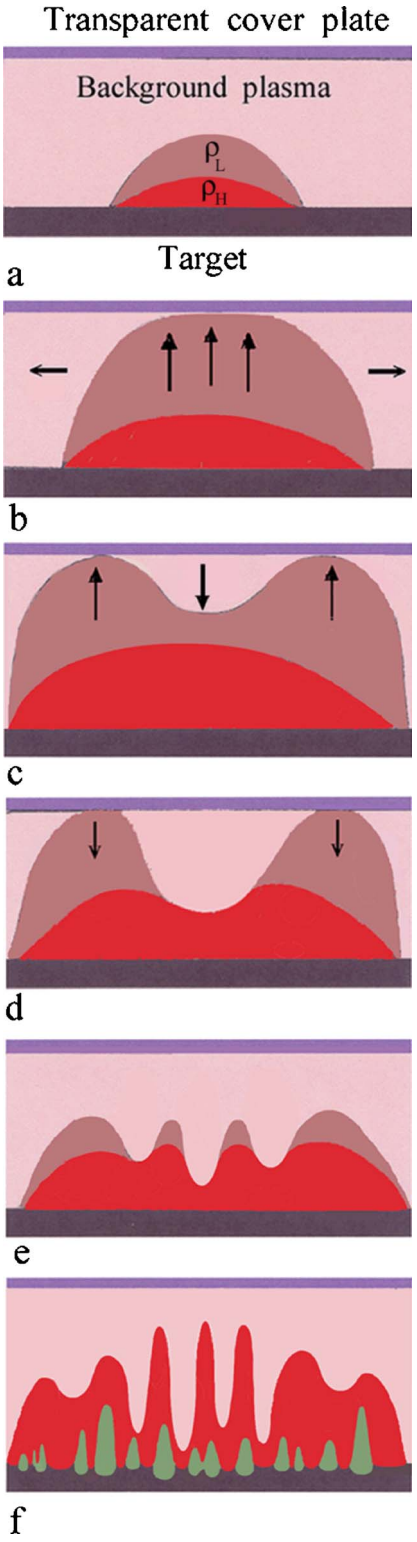

FIG. 1. (Color online) Evolution of solitary plasma waves in the semiconfined laser-matter interaction. (a) Formation of a plasma by laser ablation of the Mo target. The expanding front (1) is the front of a low-density plasma ρ_L, while front (2) is the high-density plasma layer ρ_H, which is in contact with the metal surface. (b) The expanding shock front reaches the cover plate. (c) The shock front is reflected back toward the dense plasma layer. (d) The shock front collisionally snow plows a dense plasma layer; two counterstreaming plasmas penetrate each other. (e) Behind the shock, the plasma density instability is generated in the form of plasma density oscillations at the ρ_H/ρ_L interface. The plasma instability evolves into ion acoustic solitary waves. (f) The (sub)surface spinodal explosion of bubbles in the target additionally perturbs the ρ_H/ρ_L interface. These perturbations cause a random soliton generation and soliton collisions.

with the explosion of bubbles results in the formation of microscale caverns and the spongelike metal surface.[1] The explosion of bubbles ejects monatomic vapor and small particles into the plasma layer and makes it more inhomogeneous and turbulent.

Therefore, in the SCC LMI, the plasma density interface is doubly perturbed, first, from above by the reflected shock front, and second, from below by random bubble explosions. The strong disturbance induces a very turbulent mixing and generates the collision dominated plasma ($Te/Ti \gg 1$).

In the highly collisional, dense plasma slab, the electrostatic and ion acoustic responses are highly damped and do not exist, meaning that the plasma behaves more as a classical standard fluid. The evolution of instability in such plasmatic fluid results in the generation of solitary waves and their dispersion into 1D and 2D irregular or irregular arrays of solitary pulses.

III. RESULTS AND DISCUSSION

A. Solitary plasma waves and the nanohole pattern generation

1. Irregular string of nanoholes

The SEM micrograph in Fig. 2(a) shows the irregular string of nanoholes as a fingerprint of solitary pulses. Variable depth of shallow holes in the string(s) indicates variation of intensity of solitary pulses while the variation of the hole distance concentrated about two dominant values, $d_1 \sim 1.3$ μm and $d_2 \sim 1.8$ μm, indicates variation of the interpulse distance. These characteristics indicate that solitary pulses are generated by a system that shows unstable dissipative-dispersive behavior. Such a system is described by the Benny equation,[17] which can be written in the form (Kawahara and co-workers),[16–19]

$$u_t + uu_x + \alpha u_{xx} + \beta u_{xxx} + \gamma u_{xxxx} = 0, \tag{1}$$

where α, β, and γ are positive constants characterizing instability (self-excitation), dispersion, and dissipation, respectively. In the collision-dominated plasma slab the electrons are approximately isothermal owing to the large electron thermal conductivity.[13] In such plasma slab various types of dissipative effects can occur which determine the characteristics of instability and the emerging solitary waves; various kinds of effects can be described by the dissipative coefficients through the medium. Approximations are made mostly by neglecting some dissipative coefficients or simplifying the relationships that define the coefficients. Since many parameters are involved, it is not easy to determine the interval of validity for an approximation.[14] Since plasma in the semiconfined configuration is compressed,[15] and in contrast to the above practice, we cannot neglect dissipation.

The analysis of nanoholes generated by solitary waves on the molybdenum target in the SCC LMI was based on the above Benney equation which, under periodic boundary conditions, gives a steady pulse generation. Following Kawahara, the substitution of $u \propto \exp(ikx + \omega t)$ into the linearized version of (1) gives the linear dispersion relation for ω,[17]

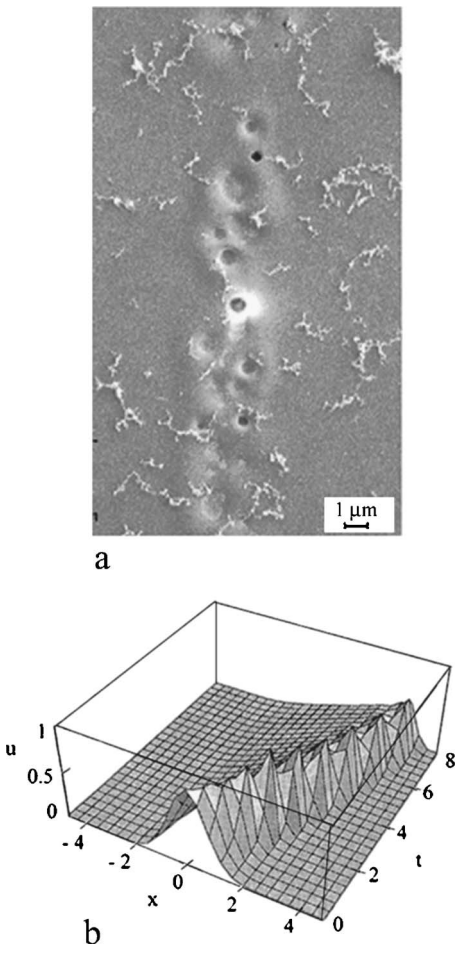

FIG. 2. Irregular string(s) of nanoholes. (a) SEM micrograph of a domain showing the irregular string of nanoholes. (b) Solitary peaks obtained by numerical simulation from the Benney equation for the Gaussian perturbation and for $\alpha = 0.01$, $\beta = 2 \times 10^{-4}$, and $\gamma = 5.066 \times 10^{-6}$.

$$\omega \propto \alpha k^2 - \gamma k^4 + i\beta k^3. \tag{2}$$

Thus, the small-amplitude sinusoidal waves are linearly unstable (growing) for long wavelengths and stable (damping) for short wavelengths.[17] Spatially periodic solutions of Eq. (1) can be obtained numerically for specific combinations of the parameters α, β, and γ.[16–19]

Therefore, the initial perturbation of the plasma slab can be described by the equations for the viscosity damped classical fluid; evolution of this perturbation gives rise to solitary waves.[20–22] The presence of strong dispersion causes the solitary waves to disperse into hump solitons. The convex target domains are in close contact with the plasma layer above the target and "feel" the effects of the plasma dynamics more intensively than the other concave ones. They are exposed to higher electron and ion temperature and to higher electron and ion density, so that hump solitons make nanohole fingerprints in these domains. However, the organization of nanoholes in these domains is different, depending on local conditions, and can be reconstructed from the solution of the Benney equation.

Numerical simulation method. The Benney equation (1) has no analytic solution so that numerical simulations are needed to get insight into the dynamics and the soliton struc-

ture. In order to make a comparative analysis of the soliton evolution in space time, the 1D Benney equation with the periodic boundary conditions was solved for three boundary intervals: (i) [0,2], (ii) [0,4], and (iii) [0,16]. The simulation was based on the numerical discretization solve (NDS) procedure which uses method of lines (MOD) for discretization of the spatial part of the equation and gives a coupled system of ordinary differential equations. Discretization was made on a very dense grid of 1000 lines in all cases. Such a fine grid was used in order to avoid coincidence between the size of the dynamic modes and the grid scale. In all simulation runs, the mode size (the hump soliton size) was much larger than the grid scale; the very fine grid scale assures that there is no numerical instability, so that the regime of validity of the calculation was not surpassed. In addition, the program used had a protection against numerical instability caused by inappropriate scale.

In the case that the mode size coincides with the grid, the program automatically switches to the finer scale, thus eliminating the grid-dependent phenomena.

Integration on a grid of a coupled system of ordinary differential equations was performed by the Runge-Kutta method. To get an insight into the influence of dispersion on the behavior of dynamic modes, i.e., the soliton behavior in space time for the collision-dominated plasma, the parameters α and γ were constant, while β was varied over a broad range of values.

The graphical presentation of the simulated hump solitons does not show all lines of the grid, but only 50, to avoid complete darkness of the graph.

The numerical simulation of string(s) of nanoholes shown in Fig. 2(b) was based on Eq. (4) using the Gaussian perturbation and the spatial mesh points with periodic boundary conditions at $x=-L,L$, with $L=4$. By using the above simulation procedure and the initial condition $u(x,0)=\cos \pi x$, a series of solitary peaks (humps) was obtained for the parameters $\alpha=0.01$, $\beta=2.00\times10^{-3}$, and $\gamma=5.066\times10^{-6}$. Solutions consisting of distinct solitonlike pulses with the same amplitude are generally observed in numerical simulations when the interval of periodicity is sufficiently long in comparison with the characteristic scale. The interval is determined by instability and dissipation and governs the width of the generated pulse. A series of solitary pulses has variable intensity; thus some of them make a very small effect (shallow circular hole), whereas the stronger ones make a slightly deeper hole, in agreement with the micrograph.

In the long-time evolutions, the interpulse distances between such pulses tend to be identical for strongly dispersive cases.[17]. By the decrease of the *dispersive effect*, these distances suddenly take distinct fixed values and then exhibit fluctuations about these values. The temporal evolution of the solutions for strongly dispersive cases is well approximated in terms of the superposition of solitonlike pulses, each of which is a steady pulse solution of the original equation. The tail structure of the pulse governs the properties of pulse interactions and thus the spatiotemporal evolutions of the wave system. Introducing the parameter $\delta[\delta=\beta/(\alpha\gamma)^{1/2}]$, which measures the relative importance of dissipation, one can estimate the characteristics of the solitary pulses.[19] When the tails are monotonic (for large δ), the pulses are mutually repelling and the final stage of the evolution is a periodic arrangement of pulses adjusted to the period of the boundary conditions of the initial value problem. When δ decreases, the oscillatory structure arises on the front-side tail of the pulse and then is enhanced. Owing to the oscillatory structure bound states arise between two pulses with definite interpulse distances.[19] Therefore, the characteristics of the string of nanoholes shown in Fig. 2(a) can be favorably interpreted on the basis of solitary humps that are the solution of the nonlinear, dispersive, and dissipative system with the Gaussian perturbation.

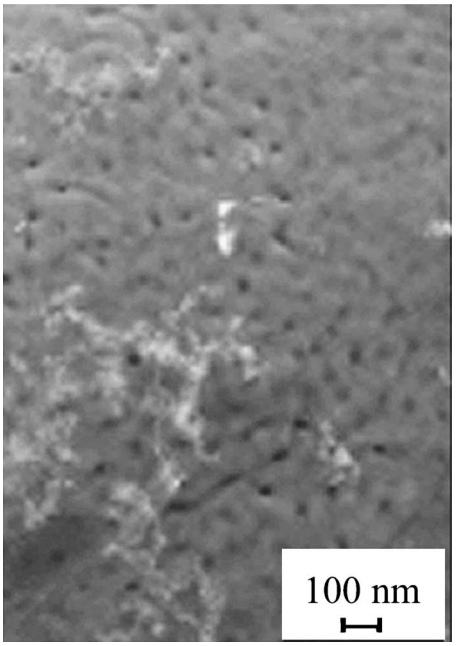

FIG. 3. SEM micrograph of a domain showing the irregular 2D array of nanoholes.

2. Irregular two-dimensional array of nanoholes

In addition to the irregular strings of holes, the SEM analysis reveals a 2D irregular pattern of nanoholes, such as shown in Fig. 3. Variation of the hole density and variation of the hole distance around some characteristic value of ~85 nm indicate that they are fingerprints of vacillating solitary plasma pulses. Numerical simulations based on the 1D Benney equation with the periodic perturbation in the [0,16], [0,4], and [0,2] intervals of periodicity reveal the transition from steepened sinusoidal perturbation into hump solitons, or the onset of chaos. The parameters α and γ are constant, while the dispersion parameter β ranges from 2.00×10^{-4} to 10.00×10^{-4}.

The evolution of hump solitons in space time as a function of dispersion, for the interval of periodicity [0,16], is shown in Fig. 4. Starting with dispersion $\beta=2.00\times10^{-4}$ the soliton amplitude reaches $A=2$ [Fig. 4(a)] and remain constant when β increases to 2.50×10^{-4} [Fig. 4(b)]. With further increase of dispersion to $\beta=3.33\times10^{-4}$ the amplitude approaches $A=3$ [Fig. 4(c)] and remain constant when dispersion increases to $\beta=5\times10^{-4}$ [Fig. 4(d)].

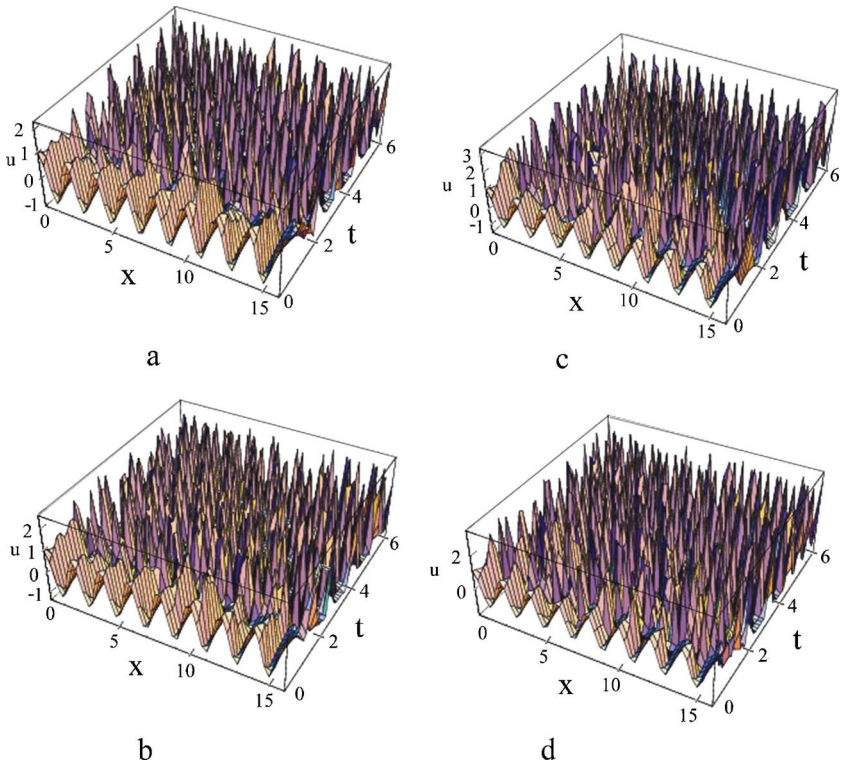

FIG. 4. (Color online) Numerically simulated evolution of the hump solitons from the initial sinusoidal perturbation as a function of the dispersion parameter β in the boundary interval $x=[0,16]$, with $\alpha=0.01$ and $\gamma=5.066\times10^{-6}$: (a) $\beta=2.00\times10^{-4}$, (b) $\beta=2.50\times10^{-4}$, (c) $\beta=3.33\times10^{-4}$, and (d) $\beta=5.00\times10^{-4}$.

More details of the soliton evolution are obtained for the shorter interval of periodicity, [0,4] (Fig. 5). The irregular soliton pattern formed at $\beta=2.00\times10^{-4}$ [Fig. 5(a)] changes and tends to an almost regular one for $\beta=3.333\times10^{-4}$ through the formation of soliton strings of gradually increasing amplitude approaching $A=3$ [Fig. 5(b)]. For $\beta=5.00\times10^{-4}$, large-amplitude oscillations appear in the soliton strings [Fig. 5(c)]. Finally, for $\beta=10.00\times10^{-4}$, the amplitude of solitons becomes almost uniform reaching $A_{\max}=6.5$, thus indicating the tendency to saturation [Fig. 5(d)].

The most detailed picture of the soliton evolution is obtained for the interval of periodicity [0,2] shown in Fig. 6. The irregular pattern obtained for $\beta=2.00\times10^{-4}$ shows solitons with the oscillatory behavior of the amplitude [Fig. 6(a)]. For $\beta=2.85\times10^{-4}$, the oscillations gradually vanish, while the amplitude increases to $A=3$, showing some regu-

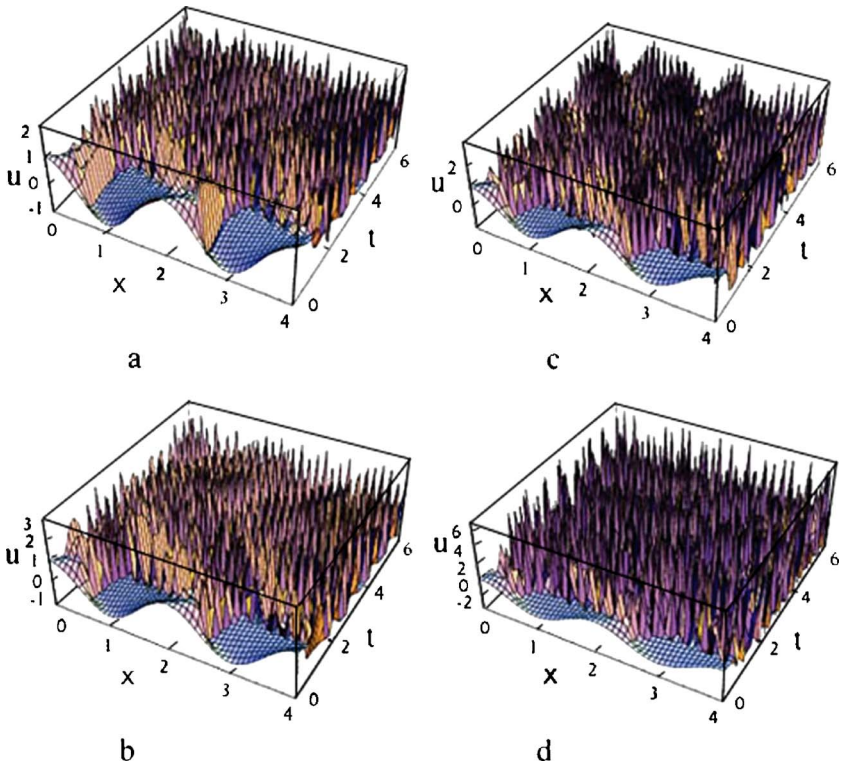

FIG. 5. (Color online) Numerically simulated evolution of the hump solitons from the initial sinusoidal perturbation as a function of the dispersion parameter β in the boundary interval $x=[0,4]$, with $\alpha=0.01$ and $\gamma=5.066\times10^{-6}$. Shorter boundary interval than in Fig. 4 gives a detailed look at the soliton characteristics: (a) $\beta=2.00\times10^{-4}$, (b) $\beta=3.33\times10^{-4}$, (c) $\beta=5.00\times10^{-4}$, and (d) $\beta=10.00\times10^{-4}$.

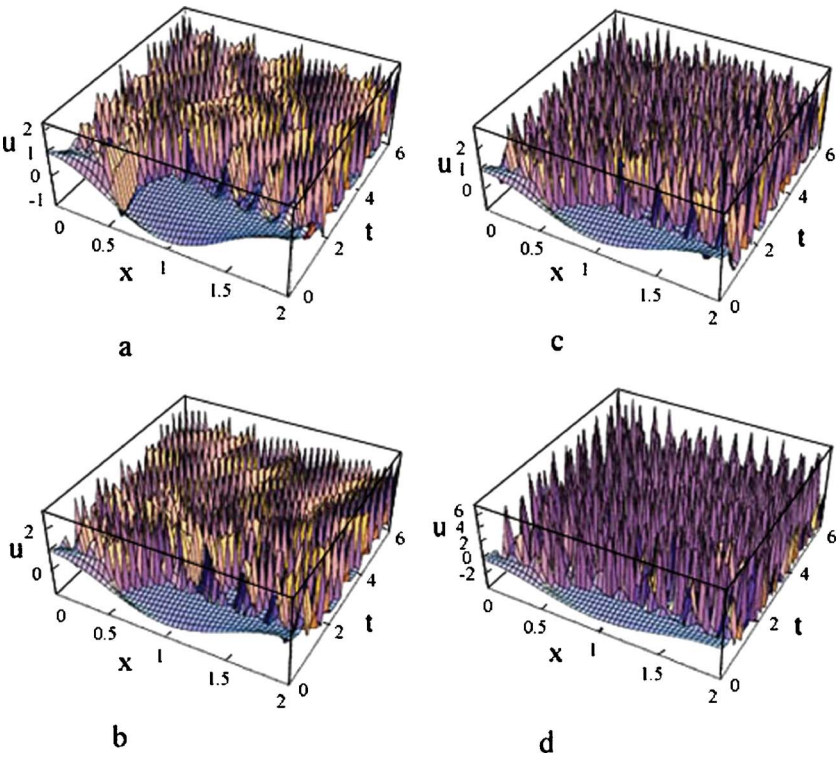

FIG. 6. (Color online) Numerically simulated evolution of the hump solitons from the initial sinusoidal perturbation as a function of the dispersion parameter β in the boundary interval $x=[0,2]$, with $\alpha=0.01$ and $\gamma=5.066\times10^{-6}$. Shorter boundary interval than in Fig. 5 reveals more characteristics of the hump solitons: (a) $\beta=2.00\times10^{-4}$, (b) $\beta=4.00\times10^{-4}$, (c) $\beta=5.00\times10^{-4}$, and (d) $\beta=10.00\times10^{-4}$.

larlike organization [Fig. 6(b)]. The tendency to regular arrangement of the soliton pattern continues with increasing dispersion and for $\beta=4\times10^{-4}$ takes the form of short strings [Fig. 6(b)]. The increase of dispersion to $\beta=5.00\times10^{-4}$ results in the formation of an almost homogeneous pattern of spikes [Fig. 6(c)]. Beyond this dispersion value (for example, at $\beta=10.0\times10^{-4}$), the pattern shows more homogenization in the hump soliton distribution, in their width, and in their amplitude (reaching $A_{max}=6.5$), characteristic of the onset of saturation [Fig. 6(d)].

Numerical simulations reveal that the hump solitons appear by decomposition of the initial periodic perturbation, for $\alpha=0.01$, $\beta=0$, and $\gamma=5.066\times10^{-6}$. Looking in the direction of the time axis in Figs. 4–6, one can see the gradual transformation of a periodic wave into irregular oscillations and finally, into separated humps that represent dispersed solitons. The decomposition of a periodic wave and the appearance of solitons occur after some time, which can be understood as a "delay time" that depends strongly on the parameters α, β, and γ and tends to zero for the parameter choice $\alpha=0.01$, $\beta=2\times10^{-3}$, and $\gamma=5.066\times10^{-6}$. Numerical simulations reveal that the formation of random hump solitons or the onset of chaos shifts to shorter times as the dispersion parameter β increases. Thus, the onset of soliton formation which for $\beta=2.000\times10^{-4}$ occurs at $t=2.2$ shifts to $t=1.2$ for $\beta=10.00\times10^{-4}$ (Table I). The solitary pulses formed at one moment do not change at the next moment, but stay mostly at the same location and are of the same intensity. However, the vacillating behavior cannot be excluded. Numerical simulations performed for the intervals of periodicity [0,16], [0,4], and finally, for [0,2] show the soliton evolution for the perturbation function with eight periods, four periods, and one period, respectively. Simulation performed with 1000 point discretization in all cases, at gradually smaller and smaller scale, represents the numerical microscope which shows more details of the soliton characteristics.

Instead of the β dependence of the soliton evolution, we consider the δ dependence, i.e., the soliton evolution as a function of a single parameter which takes into account dispersion and damping. Table I indicates that the soliton amplitude increases with δ. At the same time the soliton asymmetry which develops oscillatory structure on the front side of the pulse tail gradually increases for the higher δ values. Also, regular rows of hump solitons (the short soliton strings) that appear at $\delta=1.4778$ start to vanish and transform into an irregular hump soliton pattern at $\delta=2.6123$, indicating the onset of the intermittent deterministic-chaotic regime. The width of the hump solitons decreases with increasing δ until they transform into well-separated spikes. Besides, the soliton amplitude becomes more uniform until for $\delta=4.473$ the solitons become almost of the same size.

TABLE I. Dependence of the onset time (t) of the soliton generation from the periodic perturbation and of the soliton amplitude (A) on the dispersion (β) with constant parameters $\alpha=0.01$ and $\gamma=5.066\times10^{-6}$.

β (10^{-4})	δ	t	A
2.000	0.7807	2.2	1
2.500	1.1709	2.0	2
2.850	1.2751	1.9	3
3.333	1.4778	1.55	3
4.000	1.7715	1.50	3
5.000	2.2719	1.40	3.5
6.666	2.6123	1.3	5
10.00	4.4734	1.2	6

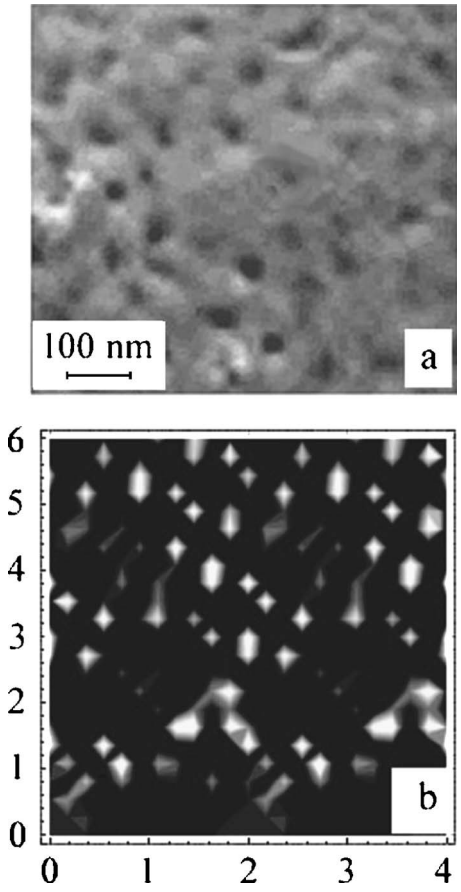

FIG. 7. (a) Comparison of the SEM micrographs of 2D irregular array of nanoholes and (b) the contour plot of the hump solitons generated for $\beta = 10.00 \times 10^{-4}$ made at the height interval {2,6}.

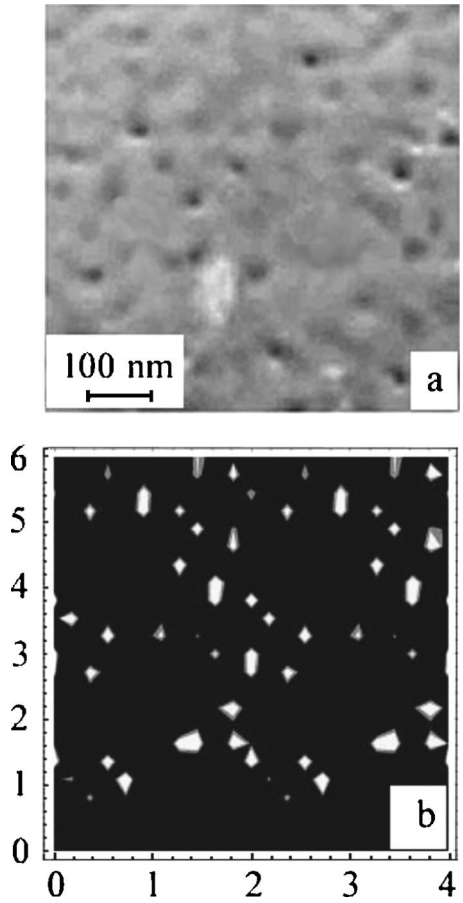

FIG. 8. (a) Comparison of the SEM micrographs of 2D irregular array of nanoholes and (b) the contour plot of the hump solitons generated for $\beta = 10.00 \times 10^{-4}$ made at the height interval {4,6.5}.

Obviously, the transitions between the almost regular and chaotic regimes are strongly dependent on δ, i.e., on the characteristic ratio of dispersion and (viscous) damping.

The characteristic of the pattern in Fig. 3 is a random 2D array of nanoholes of diameter of ~20–30 nm, which at large magnification show a cross section different from the circular one. The holes are of variable depth, ranging from very shallow to deep ones, and in this respect the pattern of nanoholes is inhomogeneous. It means that they could not be formed by the saturated solitons which have the same amplitude but by the random solitary humps of variable amplitude and of variable shape. The analysis of the micrograph (Fig. 3) gives the total nanohole density $N_{\text{total}} = 87.45 \times 10^6/\text{cm}^2$, of which $N_{\text{shallow holes}} = 51.74 \times 10^6/\text{cm}^2$ and $N_{\text{deep holes}} = 35.71 \times 10^6/\text{cm}^2$.

To make a comparison of the pattern of nanoholes and the pattern of soliton contour plots (equivalent to soliton cross section) the hump solitons were generated at a large dispersion $\beta = 10.00 \times 10^{-4}$ ($\delta = 4.4734$). The contour plots were made at three different height intervals, {0.6}, {2,6}, and {4,6.5}. The soliton contour size and their density distribution are the largest for the {0.6} height interval; they decrease for the next, {2,6}, and finally become very small for the {4,6.5} height interval. It can be seen that the contour plots ("cross sections") which are not of a regular circular shape are very similar to the shapes of the nanoholes in Figs. 7(a) and 8(a). Finally, the distribution of the nanoholes in Figs. 7(a) and 8(a) can be favorably compared with the soliton contour density distribution in Figs. 7(b) and 8(b), respectively. Thus, a 2D random pattern of nanoholes can be favorably interpreted on the basis of random solitary humps that are the solution of the nonlinear dispersive dissipative system with periodic perturbation.

3. Regular string of nanoholes

Soliton collision and formation of breather modes. In close vicinity to the domains that comprise an irregular array of holes, the domains have been observed that comprise either a regular string or a 2D array of holes. In many cases the holes are incorporated into the groove lines, as clearly seen in Fig. 9(a). The role of solitons in the formation of irregular hole patterns indicates that the regular strings and 2D arrays of nanoholes originate from the coupled solitons or breather modes. This special type of dynamic modes appears in the domains with the dominant soliton collision. Upon the collision with each other, solitons emerge with their identities unaltered except for a minor shift in position. Sometimes, all eigenvalues (self-consistent localized solution) or a subset of eigenvalues has identical real parts, corresponding to solitons moving together with the same initial velocity. Since they experience the same acceleration, they remain together forming bound state called breathers.[21–24] A breather containing many solitons in general has a symmetrical irregular shape

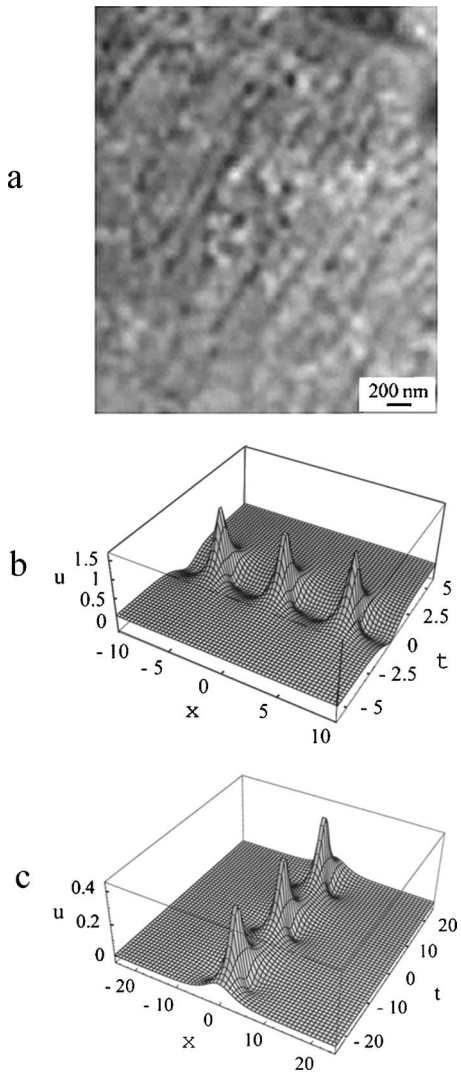

FIG. 9. Regular 1D and 2D arrays of nanoholes. (a) SEM micrograph of a domain showing the regular strings of nanoholes and the domains of 2D regular array of nanoholes. (b) Growing mode of the Boussinesq equation with $p=-1$ (after Tajiri and Watanabe (Ref. 23). (c) Stationary breather solution for $k=2/\sqrt{29}$, $\rho=0$, and $\Phi=\pi$. As seen, it is constructed as the imbricate series of rational growing modes in the t direction (after Tajiri and Watanabe (Ref. 23).

oscillating periodically in time. Under perturbation, the breather will break up and release all its solitons.[24]

For the simulation of a 1D regular string of holes shown in Fig. 9(a) caused by the breather modes, we used the Boussinesq equation (Tajiri and Murakami)[25]

$$u_{tt} - pu_{xx} - 6(u^2)_{xx} - u_{xxxx} = 0, \tag{3}$$

with $p=\pm 1$. We consider solutions of the above equation that give a 1D solitary lattice of breather modes. As shown by Tajiri and Watanabe, the substitution

$$u = u_0 \exp[i(kx - \omega t)] \tag{4}$$

gives the nonlinear evolution of an unstable mode which is exponential at the initial stage $u \sim u_0 \exp(\gamma t)\cos(kx)$, where γ is the growth rate given by $\gamma=k(k^2-p)^{1/2}$. It takes the maximum amplitude at a time and finally decays exponentially to zero $u \sim u_0' \exp(\gamma t)\cos(kx)$, which is called a growing mode. The growing mode solution can be represented in the Fourier series[23]

$$u = \sum_{n=1} 2nk^2 e^{-nkb(t)} \cos(nkx), \tag{5}$$

where

$$b(t) = (1/k)\ln\{K^{1/2}\cosh(\gamma t + \xi) + [K\cosh^2(\gamma t + \xi) - 1]^{1/2}\} \tag{6}$$

and

$$K = (4k^2 - p)/(k^2 - p), \quad \gamma = k(k^2 - p)^{1/2}. \tag{7}$$

A typical growing mode solution is shown in Fig. 9(b).

Stationary breather solution. Equation (7) with $p=-1$ has the stationary breather solution, which can be constructed from the imbricate series of rational growing modes. Such a stationary breather solution can be written as[23]

$$u = k^2\{[1 + (1/L)^{1/2}\cosh(kx + \rho)\cos(\delta t + \Phi)]/ \times[\cosh(kx + \rho) + (1/L)^{1/2}\cos(\delta t + \Phi)]^2\}, \tag{8}$$

where $L=(1-k^2)/(1-4k^2)$, $\delta=k(1-k^2)^{1/2}$, while ρ and Φ are arbitrary constants.[23]

As a nonpropagating mode, a stationary breather mode appears as a localized soliton whose amplitude increases to some maximum value and then decreases to minimum, representing the process which repeats periodically in time. A typical stationary breather solution is shown in Fig. 9(c).

Intermitted wave mode solution. The wave mode solution is constructed from a double imbricate series of rational growing modes in the form[23]

$$u(x,t) = -a^2(\Sigma_{m,n}\{1/[ax + ir(t) - (mah - 2\pi in)]^2 + 1/[ax - ir(t) - (mah - 2\pi in)]^2\} + c^2), \tag{9}$$

that is intermittent in time and space. The summation ranges over all integer pairs m and n, while a and c are some real constants; $r(t)$ is a function of t to be determined, and h is the interval in the x direction.[23]

Figure 9(a) clearly shows ~20 parallel rows with an almost regular periodic distribution of holes. Some of the holes are slightly extended and connected with the neighbor holes in the row. These characteristics of the nanohole organization can be compared with the characteristics of the 1D row of breather modes obtained by numerical simulation [Figs. 9(b) and 9(c)]. The breather modes obtained from the Boussinesq equation show the increasing width of the soliton in either one direction (x) or in two directions (x and y), as well as the existence of a soliton tail. The increasing soliton width causes two neighbor holes to appear almost joined together, thus forming a groove (with holes) as observed in Fig. 9(a). The breather mode formation based on the Boussinesq equation gives a favorable description of the 1D regular organization of nanoholes and elucidates the situation observed in some domains of the nonuniform spot.

B. Regular two-dimensional array of nanoholes

The SEM analysis reveals that some domains comprise an almost regular 2D array of nanoholes, which can be inter-

preted as a result of the 2D soliton lattice. The two-dimensional propagation of many kinds of waves in weakly nonlinear dispersive media can be described by the Kadomtsev-Petviashvili (KP) equation[21,22]

$$(u_t + 6uu_x + u_{xxx})_x + 3pu_{yy} = 0. \tag{10}$$

The KP equation is actually a two-dimensional extension of the Korteweg-deVries equation with $p=+1$. It has a solitary wave solution:[21,22]

$$u(x,t) = -(1/2)k^2 \operatorname{sech}^2[1/2(kx + ly - \omega t)], \tag{11}$$

where $\omega = k^3 + 3l^2 p/k$; k and l are the wave vectors in the x and y directions.[21,22] The conventional line soliton is stable to transverse long disturbances for the negative dispersion ($p=+1$) and unstable for the positive one ($p=-1$). Therefore, the dynamics described by the KP equation is qualitatively different, according to the type of dispersion.[21,22,25] In the case $p=-1$, various localized solitons should be formed since the line soliton is unstable to transverse disturbances. Such solitons are no longer exponential in character but take the form of rational functions in space variables.[21,22,25]

Another kind of 2D localized solitons is the periodic solution, obtained by superposition of rational soliton solutions.

Thus, the three kinds of solitons, namely, line, rational, and periodic solitons, have been known so far in the case of positive dispersion. However, the KP equation has polycnoidal wave solutions regardless of the sign of the dispersion. The double cnoidal wave is biperiodic in space, which is regarded as the superposition of two line solitons of different sizes. As Tajiri and Murakami[25] have shown, the KP equation (14) with positive dispersion gives biperiodic wave solutions (the lattice soliton solutions), which are constructed by superposition of periodic solitons or double imbricate series of rational solitons.[25] Summarizing their result, the lattice soliton solution can be obtained by superposition of an infinite number of rational solitons. Rational solitons are doubly imbricated in two (x and y) directions, giving rise to the 2D x- and y-periodic solution to the KP equation with positive dispersion.[25] Therefore, the lattice soliton solutions (a kind of 2D Toda lattice) which favorably describe the 2D regular array of nanoholes can be obtained from double imbricate series of rational solitons.

IV. CONCLUSION

Laser-matter interactions with matte Mo targets in the semiconfined configuration generate one-dimensional and two-dimensional irregular and regular arrays of nanoholes. Their origin was conjectured from the generation of solitary waves in the target plasma by the piston effect. In the semiconfined configuration, the solitary humps as the plasma density waves interact with the target surface, thus leaving the thermal/pressure fingerprints in the form of nanoholes.

The collision-dominated plasma with the presence of nonlinearity, dissipation, and dispersion under strong damping behaves as a simple fluid, most appropriately described by the Benney equation, which we used for the numerical simulation of the hump solitons. The similarity between the patterns of nanoholes and the pattern of solitons generated by numerical simulations indicates the great importance of dispersive effects in these processes. The fact that various solutions of the same equation are obtained for various types of initial perturbation indicates great inhomogeneity in the plasma-target contacts, in the variation of dispersion and dissipation parameters, as well as in the variation of perturbation conditions in the local domains of a basically random surface.

It has been shown that the irregular one-dimensional array (string) of nanoholes emerges from the irregular string of solitary peaks, which is obtained from the Benney equation for the initial perturbation of the Gaussian-type and for the periodic boundary conditions.

It has been shown that the irregular two-dimensional array of nanoholes emerges from the random solitary peaks, which are obtained from the Benney equation for the initial periodic perturbation and for the periodic boundary conditions. The regular one-dimensional string of nanoholes has been shown to emerge from the breather modes (modes formed by the soliton collision) from the Boussinesq equation. Finally, it has been indicated that the regular two-dimensional array of nanoholes emerges from the solution of the 2D Kadomtsev-Petviashvili equation.

The phenomenon of the 1D and 2D patterns of nanohole generation in the semiconfined LMI could be of great technological importance. At present, the nanohole patterns are spontaneously formed and further experimental investigation with variation of experimental conditions is needed to elucidate the underlying process in detail.

ACKNOWLEDGMENTS

One of the authors (S.L.) would like to thank Professor N. J. Zabusky, Rutgers University, New Jersey, for discussion of the solitary wave characteristics. The author is also grateful to Professor T. Kawahara, the Kyoto University (retired) for critical reading of the manuscript and valuable comments and suggestions, as well as to Dr. Y. Watanabe, the Osaka University, for discussion of the breather modes and solution of the Boussinesq equation.

[1] S. Lugomer, B. Mihaljević, G. Peto, A. Toth, and E. Horvath, J. Appl. Phys. **97**, 073305 (2005).
[2] S. Lugomer and A. Maksimović (unpublished).
[3] Y. B. Zeldowich and Y. P. Raizer, *Physics of Shock Waves and High-Temperature Hydrodynamic Phenomena* (Academic, New York, 1966).
[4] D. Lobao and A. Povitsky, AIAA J. **43**, 595 (2005).
[5] D. W. Forslund and C. R. Shonk, Phys. Rev. Lett. **25**, 1699 (1970); D. W. Forslund and J. P. Freidberg, *ibid.* **27**, 1189 (1971); D. W. Forslund, J. M. Kindel, K. Lee, and E. L. Lindman, *ibid.* **36**, 35 (1976); R. J. Mason, Phys. Fluids **15**, 845 (1972); S. O. Dean, E. A. Mc Lean, J. A. Stamper, and H. R. Griem, Phys. Rev. Lett. **29**, 569 (1977); S. A. Colgate and C. W. Hartman, Phys. Fluids **10**, 1288 (1967); S. O. Dean, E. A. McLean, J. A. Stamper, and H. R. Griem, Phys. Rev. Lett. **27**, 487 (1977).
[6] J. H. Yoo, S. H. Jeong, R. Greif, and R. E. Russo, J. Appl. Phys. **88**, 1638 (2000).
[7] S. S. Mao, X. Mao, R. Greif, and R. E. Russo, J. Appl. Phys. **89**, 4096 (2001).
[8] T. P. Wright, Phys. Rev. Lett. **28**, 268 (1972).
[9] E. C. Zeeman, *Catastrophe Theory* (Addison-Wesley, Reading, MA, 1977).
[10] T. Poston and I. Stuart, *Catastrophe Theory and its Applications* (Pitman, London, 1978).

[11]In the usual representation of the cusp catastrophe, the top sheet is the liquid phase and the bottom sheet the gaseous phase: the two catastrophes are boiling and condensation. The vertex of the cusp is the critical point at which liquid and gas exist simultaneously (Refs. 9 and 10). Grosse (Ref. 12) has shown that superheating may in principle occur for all metals, but for refractory metals (Ti, Ta, Mo, W, etc.) the cusp is large, and superheating may reach even 10^3-10^4 K.
[12]A. V. Grosse, J. Inorg. Nucl. Chem. **22**, 23 (1961).
[13]E. Ott, W. M. Manheimer, D. L. Book, and Y. P. Boris, Phys. Fluids **16**, 855 (1973).
[14]P. N. Hu, Phys. Fluids **9**, 89 (1965).
[15]R. A. Stern and J. F. Decker, Phys. Rev. Lett. **27**, 1266 (1971).
[16]T. Kawahara and M. Takaoka, Physica D **39**, 43 (1989).
[17]T. Kawahara, Phys. Rev. Lett. **51**, 381 (1983).
[18]B. F. Feng and T. Kawahara, Physica D **137**, 228 (2000).
[19]T. Kawahara and S. Toh, Phys. Fluids **31**, 2103 (1988).
[20]N. J. Zabusky and M. D. Kruskal, Phys. Rev. Lett. **15**, 240 (1965).
[21]P. G. Drazin and R. S. Johnson, *Solitons: An Introduction* (Cambridge University Press, Cambridge, 1996).
[22]M. J. Ablowitz and P. A. Clarkson, *Solitons, Nonlinear Evolutions and Inverse Scattering* (Cambridge University Press, Cambridge, 2003).
[23]M. Tajiri and Y. Watanabe, J. Phys. Soc. Jpn. **66**, 1943 (1997).
[24]M. H. Chen and C. H. Liu, Phys. Rev. Lett. **37**, 693 (1975).
[25]M. Tajiri and Y. Murakami, J. Math. Phys. **34**, 2400 (1993).